

Low-Temperature Gibbs States with Tensor Networks

Denise Cocchiarella^{1,2} and Mari Carmen Bañuls^{1,2}

¹Max-Planck-Institut für Quantenoptik, Hans-Kopfermann-Str. 1, D-85748 Garching, Germany

²Munich Center for Quantum Science and Technology (MCQST), Schellingstr. 4, D-80799 München, Germany
(Dated: January 15, 2025)

We introduce a tensor network method for approximating thermal equilibrium states of quantum many-body systems at low temperatures. In contrast to standard (thermofield double matrix product state) algorithms, our ansatz is constructed from the zero-temperature limit, the ground state, which can be simply found with a standard tensor network approach. This method allows us to efficiently compute thermodynamic quantities and entanglement properties. We demonstrate our approach within a tree tensor network ansatz, although it can be extended to other tensor networks, and present results illustrating its effectiveness in capturing the finite-temperature properties in the 1D and 2D scenario.

The Gibbs ensemble describes the state of quantum systems in equilibrium at finite temperature. Numerical techniques to approximate these states for quantum many-body systems are thus of fundamental interest. Quantum Monte Carlo methods [1] provide a powerful approach, limited, however, to models that do not suffer from the sign problem [2, 3]. Tensor networks (TNs) [4–9] offer a useful alternative. It has been shown that, at finite temperature, thermal states of local Hamiltonians satisfy an area law [10] and admit efficient TN approximations [11–13] (see also [14] for more details on the problem of approximating quantum many-body Gibbs states). In practice, many TN methods try to find thermal states via imaginary time evolution [15–17], which is used to prepare a purification of the Gibbs ensemble (the thermofield state) starting from a maximally entangled state (namely, from a maximal-rank thermal ensemble). This method usually works well at high temperatures, but accumulates error while evolving to low-temperatures, although several strategies have been developed to mitigate this [18–20]. Another drawback of this strategy is that the rank of the state is never decreased in the thermal evolution, even though at zero temperature the state should reduce to the rank-one density operator of the ground state (assuming its uniqueness). Thus, some TN methods have been introduced that use a low-rank description. Samples of minimally entangled typical thermal states (METTSs) [21–23], have proven to be effective in representing thermal properties, especially in gapped systems at temperatures well below the energy gap [24]. In Ref. [25], a single matrix product state (MPS) was constructed to represent a typical thermal state [26], and recover physical quantities with almost no sampling cost. A recent proposal used tree tensor operators (TTOs) [27] to represent low-temperature thermal states from a few individually approximated excitations. An intermediate approach is taken in [28], where the standard purification algorithm is run, but then the resulting state is approximated with a low-rank TTO.

Here we propose a method that directly targets the low

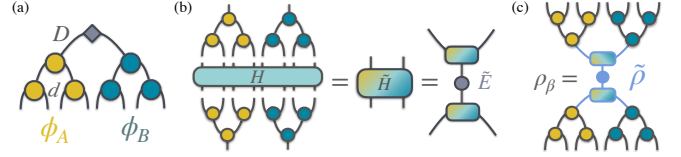


FIG. 1: Graphical representation of the proposed TN method. (a) The TTN for the ground state in canonical form with respect to a bond defines the isometries $\Phi_{A(B)}$. (b) Projecting the full Hamiltonian with them yields the corresponding effective Hamiltonian \tilde{H} . Diagonalizing the latter provides the set of eigenvalues \tilde{E} . (c) TTO representation of the thermal state, as described in Eq.(1). The unitaries diagonalizing \tilde{H} are shown as part of the tree, and the circle in the vertical bond represents the Boltzmann weights from \tilde{E} .

energy regime to construct a low-rank TN approximation starting from the zero-temperature limit, and thus is complementary to the standard imaginary time evolution. As the few-excitations ansatz using TTOs [27], it allows one to efficiently compute entropy and entanglement properties of mixed states, but it is computationally more efficient. The method is inspired by and especially suited for the properties of (near) critical systems described by a conformal field theory (CFT) [29]. The ground state of a CFT plays a key role in the creation of the conformal tower, acting as the primary state to generate excited states through specific local operators [29, 30]. Similarly, we start from the ground state to define a relevant subspace for the approximation of a thermal state. We show how the applicability of the method actually extends to more general low-temperature scenarios and check this with numerical examples in 1D and 2D models.

Gibbs state from the local effective Hamiltonian.— At finite temperature $T = 1/\beta$, the equilibrium state of a system governed by a Hamiltonian H is described by the Gibbs ensemble $\rho_\beta = e^{-\beta H}/Z = (\sum_n e^{-\beta E_n} |E_n\rangle \langle E_n|) / Z$, where $|E_n\rangle$ ($n = 0, \dots, d^N - 1$) are the energy eigenstates with energy E_n , and $Z = \text{Tr}(e^{-\beta H})$ is the partition function. At zero temperature ($\beta \rightarrow \infty$), and assuming the ground state $|E_0\rangle$ is unique, this reduces to the rank-1 density operator

$\rho_\infty = |E_0\rangle\langle E_0|$. At finite β , contributions from higher energy states are suppressed exponentially by their excess energy above the ground state, and thus at low temperatures we may expect the Gibbs state to be well approximated by a low-rank operator. In Ref. [27], such a low-rank approximation was explicitly constructed by approximating each of the few first excitations by a tree tensor network (TTN) ansatz, variationally found, and explicitly constructing their mixture with corresponding Boltzmann weights. This approach can accurately capture the behavior at very low temperatures, but becomes computationally challenging when the number of required levels increases, for instance in cases with closely spaced energies, as in critical systems. Moreover, the mixture constructed using a given number of eigenstates does not necessarily produce the best approximation with fixed rank. It is thus more desirable to have an efficient description of a relevant subspace that allows us to reconstruct the low-temperature properties. In the case of critical systems described by a CFT, such subspace could be spanned by the Schmidt vectors of the ground state, based on the observation that excited states can be expanded in this basis [31]. This suggests a method to obtain the low-rank approximation of ρ_β from the ground state of a 1D critical system. Considering a ground state and its bipartition into subsystems A and B , the corresponding Schmidt decomposition reads $|\psi_{GS}\rangle = \sum_\alpha^D \lambda_\alpha |\phi_A^\alpha\rangle |\phi_B^\alpha\rangle$, where $|\phi_{A(B)}^\alpha\rangle$ are the Schmidt vectors for the A (B) partition. They define isometries $\Phi_{A(B)}$ that map the corresponding d^{N_A} (resp. d^{N_B}) dimensional physical space to a virtual degree of freedom of dimension D . Their tensor product $U = \Phi_A \otimes \Phi_B$ is thus an isometry that maps the Hamiltonian onto the D^2 -dimensional subspace spanned by tensor products of Schmidt vectors, as $\tilde{H} = UHU^\dagger$. For a given inverse temperature β , we can then approximate the Gibbs state by that of the effective Hamiltonian \tilde{H} , embedded in the physical space as $e^{-\beta H} \approx e^{-\beta U^\dagger \tilde{H} U} = U^\dagger e^{-\beta U \tilde{H} U^\dagger} U$. This scheme is readily implementable with TTNs. We start by variationally optimizing the TTN representation of the ground state of the Hamiltonian of interest with bond dimension D , and write it in canonical form with respect to a chosen bipartition (e.g. half system, as illustrated in Fig.1(a), such that the Schmidt vectors can be directly read from the half-trees. The original Hamiltonian is then projected onto the space spanned by the products of Schmidt vectors (Fig.1(b)). Diagonalizing the projected \tilde{H} yields a set of eigenvalues $\{\tilde{E}_k\}$ and eigenvectors $\{|\tilde{E}_k\rangle\}$ where $k = 1, \dots, \chi = D^2$. An approximation to the thermal state is then obtained, as graphically shown in Fig.1(c), by

$$\rho_\beta = U^\dagger \sum_{k=0}^{\chi} \frac{e^{-\beta \tilde{E}_k}}{\tilde{Z}} |\tilde{E}_k\rangle \langle \tilde{E}_k| U = U^\dagger \tilde{\rho} U, \quad (1)$$

where $\tilde{\rho} = \left(\sum_{k=0}^{\chi} e^{-\beta \tilde{E}_k} |\tilde{E}_k\rangle \langle \tilde{E}_k| \right) / \tilde{Z}$ corresponds to

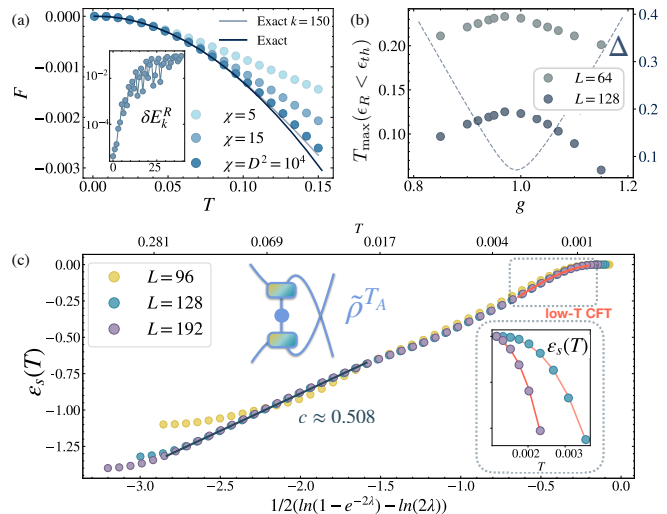


FIG. 2: Numerical results for the 1D TFI. (a) Free entropy (main plot) and relative error in energy spectrum δE_k^R (inset) at $g = 1$, $L = 128$ with open boundary conditions. Error bars (obtained comparing $D' = 70$ and $D = 100$) are smaller than the size of the markers. (b) Dependence on the field g of the maximal temperature that can be simulated while keeping the relative error in free energy below a predefined threshold $\varepsilon_{th} = 10^{-2}$. Two system sizes $L = 64, 128$ are shown (filled symbols), along with the exact energy gap Δ computed for $L = 128$ (dashed line). (c) Entanglement negativity for the critical case with periodic boundary conditions. The TN diagram (left inset) shows the partial transpose of the reduced density matrix. The right inset shows a fit of our data to the low-temperature prediction of $\varepsilon_s(T)$.

the Gibbs state of the effective local Hamiltonian and $\tilde{Z} = \sum_{k'} e^{-\beta \tilde{E}_{k'}}$. We notice that the reduced Hamiltonian \tilde{H} corresponds to the effective Hamiltonian on a bond of the tensor network. This construction is closely connected to the results in [32, 33], in which the effective Hamiltonian corresponding to one- or two-site density matrix renormalization group (DMRG) was extracted from the ground state calculation and used to access a significant part of the spectrum of the original Hamiltonian in the critical case. Our Hamiltonian, instead, is the effective one for a *zero-site* block, which corresponds to the subspace generated by the ground state Schmidt vectors.

Efficient calculation of thermal and entanglement properties. — With this construction, the thermal state is described by a low-rank mixed TTN (illustrated in Fig.1(c)). This allows the efficient computation of local or few-body observables (or sums thereof) with usual TTN contractions [7, 34]. Thermodynamic quantities can be easily obtained from the spectrum of \tilde{H} . In particular, the free energy reads $F(\rho_\beta) = \text{Tr}(H\rho_\beta) - TS(\rho_\beta) = \text{Tr}(\tilde{H}\tilde{\rho}) - TS(\tilde{\rho}) = -T \ln \tilde{Z}$, using the cyclic property of the trace and the fact that ρ_β and $\tilde{\rho}$ are related by an isometry. All the other thermodynamic properties can be then obtained starting from the free energy. This ansatz allows also access to entanglement quan-

ties, typically not accessible from the most standard purification algorithm. As an example, we show how to compute entanglement negativity. Let us consider two partitions A and B described by a density matrix ρ_{AB} , and denote by ρ^{TA} the partial transpose with respect to partition A . The entanglement negativity is defined as $\varepsilon(\rho) = \ln(2\mathcal{N}(\rho) + 1)$, where the negativity $\mathcal{N}(\rho) = \sum_{\sigma(\rho^{TA}) < 0} |\sigma(\rho^{TA})|$ is the sum of negative eigenvalues of ρ^{TA} . $\mathcal{N}(\rho)$ is positive if and only if ρ violates the positive partial transpose (PPT) condition [35–38]. While being a valid entanglement measure for mixed states, computing the negativity requires the full spectrum of ρ^{TA} , which is in general challenging. With our ansatz, the spectrum of ρ^{TA} is equivalent to the spectrum of the partial transpose of $\tilde{\rho}$, which can be computed in the reduced space (see also [27, 28]).

In the rest of the paper, we benchmark the performance of the ansatz. We find that, as can be expected, at, and near, critical points (i.e., when the energy gap is relatively small), the method works at its best. When the gap increases, the performance worsens, reflecting the fact that the ground state Schmidt vectors in this case do not capture a large enough subspace [18]. We find that the method can be improved by combining the information of further excitations above the ground state, and using the effective Hamiltonian for the highest computed one [39], we can thus interpolate between our method and the one in Ref. [27]. Finally, we apply the method to a two-dimensional system.

Numerical results in 1D.— To benchmark the method, we use the one-dimensional transverse field Ising (1D TFI) model, whose Hamiltonian reads

$$H = J \sum_{\langle i,j \rangle} \sigma_i^z \sigma_j^z - g \sum_i \sigma_i^x, \quad (2)$$

where $\langle i, j \rangle$ denotes the summation over nearest-neighbor pairs. The analytically solvable 1D TFI has a phase transition at $g_c = 1$, and thus allows us to benchmark our results in different regimes. First, comparing the free energy, shown in Fig. 2(a) for a system of size $L = 128$, $g = 1$ and open boundary conditions, with the exact result, we observe that for $D = 100$ we achieve an accuracy comparable to including the first $k = 150$ exact excitations in the mixture. We may wonder whether this corresponds to the number of individual eigenenergies that get accurately captured by \tilde{H} . However, the inset of Fig. 2 shows this not to be the case, as the relative error is already on the order of 10^{-1} after ~ 20 energy eigenvalues. Nevertheless, it is worth noticing that the first 10–12 excitations are obtained with high accuracy, and this at a low computational cost: our method requires a single run of the variational tensor network optimization, i.e., a single state, to obtain the effective Hamiltonian. In contrast, the usual strategy to obtain multiple excitations with a TN ansatz would require the sequential optimization of

each level, with overall cost scaling with the square of the number of desired excitations (for trees $\mathcal{O}(k^2 D^4)$). Our current implementation of the method fully diagonalizes \tilde{H} , with a computational cost $\mathcal{O}(D^6)$ (see [39] for details). Whereas the rank of the effective Hamiltonian can be D^2 , we can further truncate the effective Gibbs ensemble by keeping a smaller number of eigenstates χ , so that we can mimic the result of a few-excitation ansatz. The plot shows how the higher the χ , the larger the range of temperatures that are accurately described. Because $1 \leq \chi \leq D^2$, extending the temperature range even more would require increasing the bond dimension D of the ground state, which serves as a free parameter in our method. Increasing D expands the Hilbert space accessible to the Schmidt vectors, with the dimension scaling as $D^2 \times D^2$. Even though the method is inspired by CFT arguments, we can use the ansatz in other settings. To evaluate performance in such cases, we estimate the maximum temperature T_{\max} at which the relative error ϵ_R in the free energy remains below a certain threshold, ϵ_{th} , for different values of g . The results in Fig. 2(b) show that, whereas the method still performs well away from criticality, the range of valid temperatures decreases as the gap grows. Remarkably, our method allows computing entanglement quantities that can be mapped to functions in the effective subspace. In particular, we benchmark the calculation of entanglement negativity, which can be used to probe quantum critical points at finite temperature [40]. A universal scaling quantity can be constructed by subtracting from the negativity its value at $T = 0$. $\varepsilon_s(T) = \varepsilon(T) - \varepsilon(0)$, for a CFT in periodic boundary conditions, is predicted to scale (at intermediate T) as

$$\varepsilon_s(T) = \frac{c}{2} \ln \left(\frac{1 - e^{-2\lambda}}{2\lambda} \right) + f(e^{-2\lambda}), \quad (3)$$

where $\lambda = \pi l T$, l is the subsystem size and c is the central charge of the underlying CFT [40, 41]. We compare our results with the theoretical prediction in Fig. 2(c). By fitting our data to this expression, we obtain a central charge $c \approx 0.508$, in excellent agreement with the exact value $c = 1/2$. At low temperatures, a different behavior is predicted by the expansion in [40]. Our data also fit well this region, as shown by the inset of Fig. 2 and in [39]. In the opposite limit, at high temperatures, $\varepsilon_s(T)$ saturates [39], as expected from CFT predictions [40].

Numerical results in 2D.— In order to probe the more challenging two-dimensional case, we consider the TFI in Eq. (2) on a square lattice of dimension $L \times L$, for sizes up to $L = 12$. The phase diagram of the model, sketched in the inset of Fig. 3 (b), presents a finite temperature phase transition occurring at $T_c \approx 2.269$ for $g = 0$ [43] and at $g_c \approx 3.044$ for $T = 0$ [44], and has been studied in detail with Quantum Monte Carlo simulations [45]. To benchmark the method, we first consider a small system

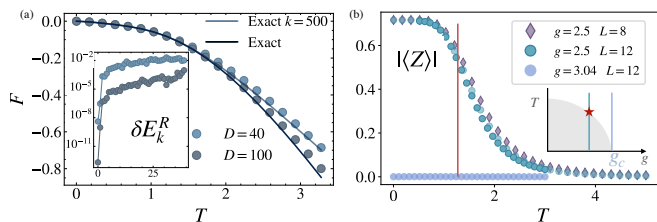


FIG. 3: Numerical results for the 2D TFI model on a $L \times L$ square lattice with periodic boundary conditions. (a) Free entropy (main plot) and relative error in energy spectrum δE_k^R (inset) at $g = 1.8$, $L = 4$, for bond dimensions $D = 40$ and 100 , compared to results from exact diagonalization in full (black solid line), or truncated to a fixed number of excitations. (b) Absolute value of the average magnetization $|\langle Z \rangle|$ as a function of temperature. Results are presented at $g = 2.5$ for $L = 8, 12$, and at $g = 3.04$ for $L = 12$. $L = 8$ is shown for $D = 70$ and $L = 12$ is shown for both $D = 100$ and $D = 70$ (shaded dots), to illustrate convergence in D . The red line indicates the expected critical temperature for $g = 2.5$ [42], and the inset shows schematically the phase diagram, with the probed values of g marked by vertical lines.

$L = 4$ at $g = 1.8$, for which the energy gap is small at this size. We compute the energy spectrum E_k and the free energy F using our method, and compare it with exact diagonalization results in Fig. 3(a). While the first few energy levels are accurately captured, we observe that the relative errors in the eigenenergies δE_k^R (shown in the inset) increase rapidly for higher levels. Nevertheless, the free energy is well-approximated in the low-temperature regime, showing that the ability of our ansatz to capture thermodynamic properties goes beyond the ability of reproducing the energy spectrum level by level.

We furthermore test the method on larger systems (up to $L = 12$) at values of the field $g = 2.5$ (for which the transition happens at $T \approx 1.2737$ [42, 45]) and $g = 3.04$ (near critical at $T = 0$). Fig. 3(b) shows the temperature dependence of the average magnetization $|\langle Z \rangle| = |\frac{1}{N} \sum_i \sigma_i^z|$, which acts as an order parameter. At $g = 3.04$ we find the order parameter to vanish at all T , as the system is in the disordered phase at any T . Further from the critical point, at $g = 2.5$, we observe the magnetization decaying as temperature grows, from a plateau at small T (converged in system size) to a vanishing value at high temperatures, consistent with a disordered phase. Rather than an abrupt drop, as expected in the thermodynamic limit, we obtain a smooth variation for the finite system, but becoming sharper as L increases, and compatible with the literature [42, 46].

Discussion.— We have presented a method to obtain a low-rank tensor network approximation of the thermal equilibrium state of a quantum many body system at low temperatures, starting from the zero-temperature limit and thus complementing the standard imaginary time evolution approach. This approach is inspired by CFT arguments: as the ground state acts as a primary state to generate excited states through specific local operators, we start from the Schmidt vectors of the ground

state to define a relevant subspace for the approximation of a thermal state. Our numerical results show how the applicability of the method actually extends to more general low-temperature scenarios and higher dimensions. While the performance degrades as the gap opens, it is possible to improve the results by constructing a mixture of our ansatz, computed from an excited state, and lower single excitations components [39], in a way interpolating between our method and that in Ref. [27]. Our method enables the efficient computation of thermodynamic and entanglement properties. Compared to other multi-excitation methods, we find that our method produces a better approximation with fixed rank at a comparably lower computational effort. We have presented the algorithm for tree tensor networks, which allows us to study finite 2D systems, with different geometries and boundary conditions, despite not inherently fulfilling an area law. MPS can straightforwardly be used as a particular case of TTN, but an extension for other TN ansatzes (as general or restricted PEPS) could also be possible. Our method is valid for finite sizes as, in the thermodynamic limit, the ansatz reduces to a state with vanishing energy density. It would thus be interesting to explore whether it can be extended to encompass states with finite energy density in such limit, while maintaining some of the computability properties. Whereas we focused here on the properties of the ansatz in different settings, practical applications may include the exploration of very-low T thermal phase transitions in 2D systems, or critical fan regimes [47] in 1D.

We thank J. I. Cirac, Y. Liu, T. Roscilde and C. Hotta for inspiring discussions and pointing us to relevant references. This work was partially supported by the Deutsche Forschungsgemeinschaft (DFG, German Research Foundation) under Germany's Excellence Strategy – EXC-2111 – 390814868; and Research Unit FOR 5522 (grant nr. 499180199), and by the EU-QUANTERA project TNiSQ (BA 6059/1-1).

Raw data are available on Zenodo [48].

-
- [1] A. W. Sandvik, Computational studies of quantum spin systems, in *AIP Conference Proceedings*, Vol. 1297 (American Institute of Physics, 2010) pp. 135–338.
 - [2] E. Loh Jr, J. Gubernatis, R. Scalettar, S. White, D. Scalapino, and R. Sugar, Sign problem in the numerical simulation of many-electron systems, *Physical Review B* **41**, 9301 (1990).
 - [3] M. Troyer and U.-J. Wiese, Computational complexity and fundamental limitations to fermionic quantum monte carlo simulations, *Phys. Rev. Lett.* **94**, 170201 (2005).
 - [4] F. Verstraete, V. Murg, and J. I. Cirac, Matrix product states, projected entangled pair states, and variational renormalization group methods for quantum spin systems, *Adv. Phys.* **57**, 143 (2008).
 - [5] U. Schollwöck, The density-matrix renormalization group

- in the age of matrix product states, *Ann. Phys.* **326**, 96 (2011).
- [6] R. Orús, A practical introduction to tensor networks: Matrix product states and projected entangled pair states, *Annals Phys.* **349**, 117 (2014).
- [7] P. Silvi, F. Tschirsich, M. Gerster, J. Jünemann, D. Jaschke, M. Rizzi, and S. Montangero, *The Tensor Networks Anthology: Simulation techniques for many-body quantum lattice systems*, *SciPost Physics Lecture Notes*, 008 (2019).
- [8] K. Okunishi, T. Nishino, and H. Ueda, Developments in the Tensor Network — from Statistical Mechanics to Quantum Entanglement, *J. Phys. Soc. Jpn* **91**, 062001 (2022).
- [9] M. C. Bañuls, *Tensor Network Algorithms: A Route Map*, *Annu. Rev. Condens. Matter Phys* **14**, 10.1146/annurev-conmatphys-040721-022705 (2023).
- [10] M. M. Wolf, F. Verstraete, M. B. Hastings, and J. I. Cirac, Area laws in quantum systems: Mutual information and correlations, *Phys. Rev. Lett.* **100**, 070502 (2008).
- [11] M. B. Hastings, Solving gapped hamiltonians locally, *Phys. Rev. B* **73**, 085115 (2006).
- [12] M. Kliesch, C. Gogolin, M. J. Kastoryano, A. Riera, and J. Eisert, Locality of temperature, *Phys. Rev. X* **4**, 031019 (2014).
- [13] A. Molnar, N. Schuch, F. Verstraete, and J. I. Cirac, Approximating gibbs states of local hamiltonians efficiently with projected entangled pair states, *Phys. Rev. B* **91**, 045138 (2015).
- [14] Á. M. Alhambra, Quantum many-body systems in thermal equilibrium, *PRX Quantum* **4**, 040201 (2023).
- [15] F. Verstraete, J. J. García-Ripoll, and J. I. Cirac, Matrix product density operators: Simulation of finite-temperature and dissipative systems, *Phys. Rev. Lett.* **93**, 207204 (2004).
- [16] M. Zwolak and G. Vidal, Mixed-state Dynamics in One-Dimensional Quantum Lattice Systems: A Time-Dependent Superoperator Renormalization Algorithm, *Physical Review Letters* **93**, 207205 (2004).
- [17] A. E. Feiguin and S. R. White, Finite-temperature density matrix renormalization using an enlarged hilbert space, *Phys. Rev. B* **72**, 220401 (2005).
- [18] B.-B. Chen, L. Chen, Z. Chen, W. Li, and A. Weichselbaum, Exponential thermal tensor network approach for quantum lattice models, *Physical Review X* **8**, 031082 (2018).
- [19] T. Munehisa, An improved finite temperature Lanczos method and its application to the spin-1/2 Heisenberg model on the kagome lattice, *World Journal of Condensed Matter Physics* **4**, 134 (2014).
- [20] Q. Li, Y. Gao, Y.-Y. He, Y. Qi, B.-B. Chen, and W. Li, Tangent space approach for Thermal Tensor Network Simulations of the 2D Hubbard Model, *Phys. Rev. Lett.* **130**, 226502 (2023).
- [21] S. R. White, Minimally entangled typical quantum states at finite temperature, *Phys. Rev. Lett.* **102**, 190601 (2009).
- [22] E. Stoudenmire and S. R. White, Minimally entangled typical thermal state algorithms, *New Journal of Physics* **12**, 055026 (2010).
- [23] A. Sinha, M. M. Rams, and J. Dziarmaga, Efficient representation of minimally entangled typical thermal states in two dimensions via projected entangled pair states, *Phys. Rev. B* **109**, 045136 (2024).
- [24] M. Binder and T. Barthel, Minimally entangled typical thermal states versus matrix product purifications for the simulation of equilibrium states and time evolution, *Phys. Rev. B* **92**, 125119 (2015).
- [25] A. Iwaki, A. Shimizu, and C. Hotta, Thermal pure quantum matrix product states recovering a volume law entanglement, *Phys. Rev. Res.* **3**, L022015 (2021).
- [26] S. Sugiura and A. Shimizu, Thermal pure quantum states at Finite Temperature, *Phys. Rev. Lett.* **108**, 240401 (2012).
- [27] L. Arceci, P. Silvi, and S. Montangero, Entanglement of formation of mixed many-body quantum states via tree tensor operators, *Phys. Rev. Lett.* **128**, 040501 (2022).
- [28] N. Reinić, D. Jaschke, D. Wanisch, P. Silvi, and S. Montangero, Finite-temperature Rydberg arrays: Quantum phases and entanglement characterization, *Physical Review Research* **6**, 033322 (2024).
- [29] P. Francesco, P. Mathieu, and D. Sénéchal, *Conformal field theory* (Springer Science & Business Media, 2012).
- [30] B. Herwerth, G. Sierra, H.-H. Tu, and A. E. B. Nielsen, Excited states in spin chains from conformal blocks, *Phys. Rev. B* **91**, 235121 (2015).
- [31] In preparation, (2025).
- [32] A. A. Eberharter, L. Vanderstraeten, F. Verstraete, and A. M. Läuchli, Extracting the speed of light from matrix product states, *Phys. Rev. Lett.* **131**, 226502 (2023).
- [33] N. Chepiga and F. Mila, Excitation spectrum and density matrix renormalization group iterations, *Phys. Rev. B* **96**, 054425 (2017).
- [34] Y.-Y. Shi, L.-M. Duan, and G. Vidal, Classical simulation of quantum many-body systems with a tree tensor network, *Phys. Rev. A* **74**, 022320 (2006).
- [35] A. Peres, Separability criterion for density matrices, *Phys. Rev. Lett.* **77**, 1413 (1996).
- [36] R. Horodecki and M. Horodecki, Information-theoretic aspects of inseparability of mixed states, *Phys. Rev. A* **54**, 1838 (1996).
- [37] R. Horodecki, P. Horodecki, M. Horodecki, and K. Horodecki, Quantum entanglement, *Rev. Mod. Phys.* **81**, 865 (2009).
- [38] G. Vidal and R. F. Werner, Computable measure of entanglement, *Phys. Rev. A* **65**, 032314 (2002).
- [39] See Supplemental Material.
- [40] P. Calabrese, J. Cardy, and E. Tonni, Finite temperature entanglement negativity in conformal field theory, *Journal of Physics A: Mathematical and Theoretical* **48**, 015006 (2014).
- [41] H. Shapourian and S. Ryu, Finite-temperature entanglement negativity of free fermions, *Journal of Statistical Mechanics: Theory and Experiment* **2019**, 043106 (2019).
- [42] P. Czarnik and P. Corboz, Finite correlation length scaling with infinite projected entangled pair states at finite temperature, *Phys. Rev. B* **99**, 245107 (2019).
- [43] L. Onsager, Crystal statistics. i. a two-dimensional model with an order-disorder transition, *Phys. Rev.* **65**, 117 (1944).
- [44] P. Pfeuty and R. J. Elliott, The Ising model with a transverse field. ii. ground state properties, *Journal of Physics C: Solid State Physics* **4**, 2370 (1971).
- [45] S. Hesselmann and S. Wessel, Thermal ising transitions in the vicinity of two-dimensional quantum critical points,

Phys. Rev. B **93**, 155157 (2016).

- [46] P. Czarnik, L. Cincio, and J. Dziarmaga, Projected entangled pair states at finite temperature: Imaginary time evolution with ancillas, Phys. Rev. B **86**, 245101 (2012).
- [47] I. Frérot and T. Roscilde, Reconstructing the quantum critical fan of strongly correlated systems using quantum correlations, Nature Communications **10**, 577 (2019).
- [48] D. Cocchiarella and M. C. Bañuls, Low-temperature gibbs states with tensor networks (2024).

SUPPLEMENTAL MATERIAL

Convergence of the Method

The convergence of tensor network methods can be evaluated by systematically increasing the bond dimension D of the tensors in the network. As D grows, the solution becomes more accurate, but computationally more expensive. If the Schmidt vectors of the ground state $|\psi_{GS}\rangle = \sum_{\alpha} \lambda_{\alpha} |\phi_A^{\alpha}\rangle |\phi_B^{\alpha}\rangle$ form a complete basis, the isometry defined as $U = \Phi_A \otimes \Phi_B$ is a unitary matrix, and our ansatz will converge to the exact result. However, practical convergence is limited by the physical properties of the system under consideration. At critical points, the Schmidt values typically decay algebraically, allowing for better convergence with increasing D compared to gapped systems, where Schmidt values decay exponentially. In this case the ground state may not span the entire Hilbert space, as a finite D can already capture the essential physics of the system. Artificially increasing D beyond the rank of the ground state might enlarge the isometry, but the additional singular vectors are no longer derived from the ground state. Consequently, the improvement is not guaranteed to be smooth or systematic as D approaches its exact value.

In practice, we increase the bond dimension D of the TTN until results are converged within a predefined precision. Fig. 4 shows, as a concrete example, the convergence of the entanglement negativity and free energy (inset) with bond dimension for a system of size $L = 128$, at the critical point $g = 1$.

In order to evaluate the performance of the method when the exact solution is known, we establish a relative error threshold $\epsilon_{th} = 0.01$ for the free energy and define $T_{max}(\epsilon_R < \epsilon_{th})$ as the maximum temperature at which the relative error ϵ_R in the free energy remains below ϵ_{th} , as shown in Fig. 2(b) in the main text.

Computational cost of the algorithm

We summarize the computational costs of the algorithm's key steps, focusing on their scaling with the bond dimension D . A more detailed understanding of these estimates can be obtained by referring to the TTN framework described in [7].

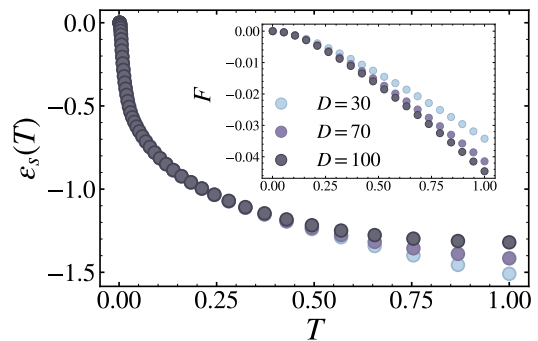


FIG. 4: Convergence of the results with bond dimension as a function of temperature, for the 1D TFI at $g = 1$, $L = 128$. The upper panel shows entanglement negativity in PBC, while the lower panel shows the free energy in OBC, for the same set of bond dimensions.

- Ground state search and creation of the bond-0 effective Hamiltonian \tilde{H} : The ground state search is performed iteratively by optimizing individual tensors in the network. Once the ground state is obtained, the bond-0 effective Hamiltonian \tilde{H} is constructed. The computational cost is dominated by the most expensive tensor contraction in these steps, scaling as $\mathcal{O}(D^4)$.
- Diagonalization of \tilde{H} : \tilde{H} is a $D^2 \times D^2$ matrix. In the current version of the proposed method, we have fully diagonalized \tilde{H} , therefore the cost of this step is $\mathcal{O}(D^6)$. If only few energies are needed, the cost can be reduced to $\mathcal{O}(D^4)$.
- Entanglement negativity: this step involves two main computational processes. First, the partial transposition of the density matrix, which scales as $\mathcal{O}(D^4)$, and second, the spectrum of the partially transposed matrix, which has a higher computational cost of $\mathcal{O}(D^6)$.
- Expectation values: Computing the expectation value of a local observable acting on a specific site requires the contraction of only three tensors, provided the TTN is center-gauged to the tensor associated with that site. This computation is independent of the system size N and scales as $\mathcal{O}(D^4)$.

Far from criticality: an improved method

As discussed in the main text, and intuitively expected from the CFT motivation of our approach, the performance of the method decreases for gapped systems. For instance, if we consider the case $g = 1.5$, at which the gap is significant, we find the temperature threshold at $T_{max} \approx 0.03$ (for $L = 128$), to be compared to $T_{max} \approx 0.12$ for the critical $g = 1$. This reflects the fact that the ground state Schmidt vectors in this case do

not capture a large enough subspace [33]. At the same time, in this case a smaller bond dimension suffices to capture accurately the ground state and a few excitations. We may thus improve our method by combining it with a multi-excitation ansatz in the spirit of Ref. [27]. More concretely, we could find a few of the lowest-energy eigenstates by the recurrent variational optimization, and combine their Boltzmann-weighted individual contributions to the thermal state with that of an effective Hamiltonian obtained from a state different from the ground state. To test this idea, we find the ground and first excited state variationally, and write the improved ansatz (up to normalization) as

$$\rho_\beta \propto e^{-\beta E_0} |E_0\rangle \langle E_0| + U_1^\dagger \left(\sum_{k=1}^{\chi} e^{-\beta \tilde{E}_k^{(1)}} |\tilde{E}_k^{(1)}\rangle \langle \tilde{E}_k^{(1)}| \right) U_1, \quad (4)$$

where U_1 and $\tilde{E}_k^{(1)}$ are defined in terms of the effective Hamiltonian obtained from the first excitation. As shown in Fig. 5, this improves the performance moderately. We have compared the standard and improved method with exact results. First, we notice that this improved method yields a lower value of the free energy than the first version of the method (using only the ground state). We check that the improvement does not simply correspond to having two very accurate estimates for the first two energy levels, as keeping only these two levels, but exactly computed, produces a worse value of the free energy than even our original method (see Fig. 5). Using the modified ansatz (4) seems comparable, instead, to having five exactly computed excitations, in this case. By increasing the number of individual excitations, and using the effective Hamiltonian for the highest computed one, we can thus interpolate between our method and the one in [27]. Interestingly, we find that a similarly accurate estimate of the free energy is obtained using only the information from the first excited state, i.e. $\rho_\beta \propto U_1^\dagger e^{-\beta \tilde{H}_1} U_1$, where \tilde{H}_1 is obtained projecting the Hamiltonian with the Schmidt isometries from the first excited state. We observe that the spectrum of \tilde{H}_1 also captures the ground state energy E_0 with good accuracy.

Entanglement negativity at low and high temperature: fit from predictions

In the next paragraphs, we provide details about the fits for the entanglement negativity shown in the main text. In [40], a universal scaling form for the finite tem-

perature negativity was derived. In the limit of low ($T \ll l$, where T is the temperature and l is the subsystem size) and high temperatures ($T \gg l$), the expansion of this universal form can be obtained by means of the operator product expansion (OPE). At high-temperature, the negativity attains a constant non-universal value.

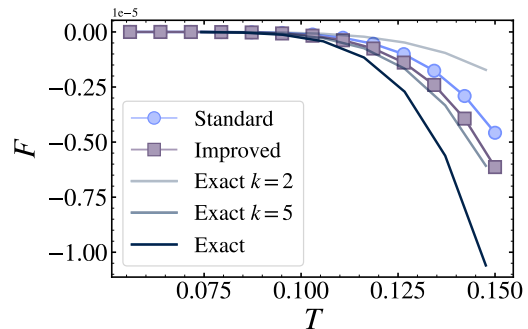


FIG. 5: Performance of the method in the gapped regime, and improved ansatz. The figure shows the free energy as a function of temperature for the 1D TFI at $g = 1.5$, for $L = 96$, using $D = 100$, for our original ansatz (blue circles) and the improved one in (4) (squares). Solid lines indicate the result from a fixed number k of exactly computed excitations, from $k = 2$ (lightest grey, less accurate than our ansatz), to $k = 5$ (comparable to the improved ansatz) and the full exact result (black line, for reference).

The study of the approach to this constant value requires the knowledge of the subleading terms in the OPE, a more involved analytical calculation. It is remarkable that our data finds the saturation naturally, as can be appreciated in Fig. 4. At intermediate T , CFT predicts [40, 41] the behavior shown in Eq. (3). Fitting our data to this formula, we indeed recover the central charge value $c = 0.508$, in good agreement with the theoretical $c = 0.5$. At low-temperature, the contribution to the negativity is of the form

$$\varepsilon_s(T) = \frac{c(\pi l T)^2}{12} + C_k (l T)^{4\Delta_k} + \dots \quad (5)$$

The first contribution to this expression is analytic and comes from the stress-energy tensor. The second, is a non-analytic and non-trivial term. The constant C_k is undetermined, and Δ_k is a scaling dimension [40]. Understanding which contribution is more relevant depends on the precise operator content of the theory and is indeed an interesting check [40]. Our method allows us to directly extract these terms numerically, from the fit of our computed data to the expression in Eq. (5). In particular, we obtain for $L = 128$, $\Delta_k \sim 0.76$, and for $L = 192$, $\Delta_k \sim 0.8$ whilst $C_k \sim -4.6$ for $L = 128$, and $C_k \sim -5.7$ for $L = 192$, as reported in Fig. 6.

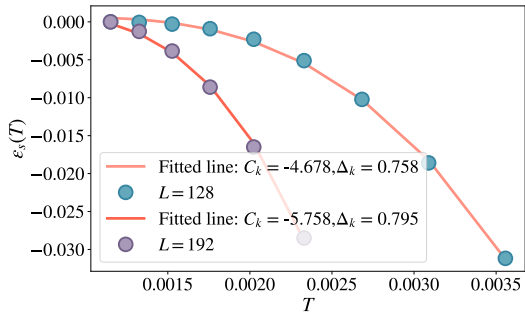


FIG. 6: Low-temperature behavior of the entanglement negativity. We show our data for $L = 128$ (blue circles) and $L = 192$ (purple circles), and the corresponding fits to Eq. (5) (orange lines), for the 1D TFI at criticality.